

Functionalised [Ge₉Ni] Clusters as Homogeneous Single-Site Catalysts for Olefin Isomerisation Reactions

Nicole S. Willeit,^[a, b] Wilhelm Klein,^[a] Peter Coburger,^[a] Elke Fritz-Langhals,^[a] and Thomas F. Fässler^{*[a, b]}

Single-site catalysis is an increasingly vital strategy to optimise heterogeneous catalytic reactions. In an ideal case, the nature and the population of catalytically active sites are all identical, which is impossible to realise on a solid support. The idea of single site catalysts is transferred from heterogeneous to homogeneous catalysis by the incorporation of a transition metal with oxidation state 0 in the surface of a small, soluble, molecular, homoatomic germanium atom cluster that also comprises main group atoms with oxidation state close to zero. An optimised synthetic protocol for four cluster compounds Hyp₃Et[Ge₉Ni]PR₃ (R = Ph, ^tolyl, ⁱPr, Me) is presented, in which the transition metal is embedded in Ge atoms of a polyhedral cluster. The products were characterised by NMR spectroscopy, LIFDI/MS and elemental analysis and also structurally characterised for R = ⁱPr and Me by single crystal X-ray structure determination comprising a *closo*-[Ge₉Ni] core. The catalytic

potential is investigated for various olefin isomerisation reactions. The formation of an active metal site is realized by ligand dissociation, which is observed for PPh₃. DFT calculations of Hyp₃Et[Ge₉Ni]PR₃ (R = Ph, ⁱPr, Me), Hyp₃Et[Ge₉Ni](tolyl) and Hyp₃Et[Ge₉Ni](C₆H₁₁) show that ligand exchange with substrate molecules occurs during the catalytic reaction. Since the same principle, namely a bare metal atom site at the cluster surface, applies as in single-site heterogeneous catalysis and since in contrast to classical homogeneous catalysis the metal atom is embedded in a cluster surface, the abbreviation *SSHoC* for Single Site Homogeneous Catalyst is proposed for this catalyst type. Since each metal atom is catalytically active, *SSHoC* enable a considerable increase in efficiency of catalysts and thus allow for sustainable use of expensive and less abundant transition metals.

Introduction

Single-site catalysts are an emerging field in heterogeneous catalysis and are known to catalyse various chemical reactions, such as hydrogenations, oxidations, hydroformylations, polymerisations or isomerisation. Generally, single atom sites (active centres) are placed on a support for heterogeneous catalytic reactions (*SSHC* = single site heterogeneous catalysts). A large category of *SSHC* includes individual isolated atoms that are anchored to high-area supports such as silica. A large variety of metals have been grafted on surfaces but mainly of oxides, and thus the metal atom adopts higher oxidation states. In addition,

even though using the right synthetic tools and the designed catalyst structure is well-defined, not all active sites will be structurally identical.^[1–5] Based on this catalyst class, we planned to create a similar structural motif by i) specifically incorporating an accessible low valent transition metal that ii) binds to a non-oxide support, and iii) that allows for a truly molecular understanding and for a uniform and well-defined free coordination site. We propose that the stabilisation of low-valent transition metal atoms can be best realised if they bind to a non-oxide support. We found that such a combination of properties can be realised by using homoatomic molecular main-group element clusters as a support with the advantage that the resulting cluster-metal complexes are also soluble, thus allowing to transfer the *SSHC* concept to *SSHoC*, a *single site homogeneous catalyst*. Small homoatomic clusters with a uniform size of nine atoms are accessible for the elements Si–Pb.^[6–8] Among those, the polyanion [Ge₉]^{4–} is the one that is best investigated, and recently it has been shown that germanium atom clusters form uncharged species by adding up to four ligands.^[9–10] [Ge₉] clusters are readily accessible through the binary phase K₄Ge₉ by simply fusing the elements at elevated temperatures.^[11–12] Reaction of [Ge₉]^{4–} with chloro-silanes lead to functionalized clusters [Hyp₂Ge₉]^{2–} and [Hyp₃Ge₉][–] (Hyp = Si(TMS)₃).^[13–14] Neutral clusters are realised by reacting K[Hyp₃Ge₉] with organotin halides, acid chlorides or halogenated hydrocarbons.^[15–18]

Several reactions of functionalised clusters with transition metals have been reported in recent years. K[Hyp₃Ge₉] forms with ^{DiPP}NHC-*M*-complexes (*M* = Cu, Ag, Au) [Hyp₃Ge₉MNHC^{DiPP}],

[a] N. S. Willeit, Dr. W. Klein, Dr. P. Coburger, Dr. E. Fritz-Langhals, Prof. Dr. T. F. Fässler
 Department of Chemistry
 TUM School of Natural Sciences
 Technical University of Munich (TUM)
 Lichtenbergstraße 4, D-85748 Garching (Germany)
 E-mail: thomas.faessler@lrz.tum.de
 Homepage: <http://www.ch.nat.tum.de/acnm>

[b] N. S. Willeit, Prof. Dr. T. F. Fässler
 Wacker Institute of Silicon Chemistry
 Technical University of Munich (TUM)
 Lichtenbergstraße 4, D-85748 Garching (Germany)

 Supporting information for this article is available on the WWW under <https://doi.org/10.1002/cctc.202301200>

 © 2023 The Authors. ChemCatChem published by Wiley-VCH GmbH. This is an open access article under the terms of the Creative Commons Attribution License, which permits use, distribution and reproduction in any medium, provided the original work is properly cited.

wherein the metal atom overcaps one of the triangular surfaces of the $[\text{Ge}_9]$ core.^[19] Similarly, Ni, Zn, and Cu atoms bind to the cluster forming $[\text{Hyp}_3\text{Ge}_9\text{ML}]$ ($M/L = \text{Ni}/\text{dppe}$, Zn/Cp^* , $\text{Cu}/\text{P}^i\text{Pr}_3$, MIC, CAAC) complexes (Figure 1a).^[20–21] Bridging metal atoms occur in $[\text{Hyp}_3\text{Ge}_9\text{MGe}_9\text{Hyp}_3]^{3-}$ ($M/a = \text{Mn}/0$, $\text{Pd}/2$, Cu , Ag , $\text{Au}/1$, Zn , Cd , $\text{Hg}/0$)^[22–25] and the oligomers $[\text{Hyp}_3\text{Ge}_9\text{CuGe}_9\text{Hyp}_3\text{CuPPh}_3]^{24}$ and $[\text{TMS}_3\text{ZnHyp}_3\text{Ge}_9\text{PtGe}_9\text{Hyp}_3\text{ZnTMS}_3]$.^[26] Thereby the structure is analogous to Figure 1a, but with L being another Ge_9 cluster, so the metal has an overall η^6 -coordination. Whereas these clusters are best described as η^3 -ligands coordinating to the transition metal, cluster framework expansions are also known. In $[\text{Hyp}_3\text{Ge}_9\text{M}(\text{CO})_3]^-$ ($M = \text{Cr}$, Mo , W), the metal atoms result as an apex of a Ge_4 square, thus being part of the deltahedral *closo*-cluster forming a bicapped square antiprism (Figure 1b).^[27–28] Reaction of $[\text{Hyp}_3\text{Ge}_9]^-$ with $[\text{RhCODCl}]_2$ leads to uncharged $\text{Hyp}_3[\text{Ge}_9\text{Rh}]\text{COD}$ having an analogous structure but now bearing the metal atom in the capping position (Figure 1c). It was shown that the Rh atom, even fully coordinated, is capable of catalysing the hydrogenation of cycloocta-1,5-diene (COD) and 1-hexene.^[29–30] Uncharged molecular clusters are further accessible through cluster expansion of $[\text{Hyp}_3\text{EtGe}_9]$ with $\text{Pd}(\text{PPh}_3)_4$ to gain $\text{Hyp}_3\text{Et}[\text{Ge}_9\text{Pd}]\text{PPh}_3$.^[31] The analogous structures with Ni and Pt were realised through reaction with $\|\text{-M}(\text{PPh}_3)_2$ ($M = \text{Ni}$, Pt).^[32] In all three cases, ten-atomic $[\text{Ge}_9\text{M}]$ deltahedra result, with the metal atom located in the square of the bicapped square antiprism (Figure 1b). These examples confirm the possible metalation of Ge_9 *Zintl* clusters and make them promising candidates for application in catalytic reactions.

In addition to the above mentioned *Zintl* type clusters, there are the so-called siliconoids, which are unsaturated silicon clusters.^[33] These compounds can also be extended with transition metals, with the siliconoid acting more as a ligand, analogous to benzene. Recently, an iridium-extended siliconoid was shown to be active in alkene isomerisation.^[34] This, in turn, underlines the catalytic potential of metalated cluster compounds.

Herein, we report a new synthetic approach to ten-atomic *closo*- $[\text{Ge}_9\text{Ni}]$ clusters allowing for a more general synthetic strategy to uncharged metalated clusters and thus for a variation of the phosphine ligand (PPh_3 , P^tolyl_3 , P^iPr_3 and PMe_3). Since it is known that only the Ni species shows dynamic processes in solution in contrast to the analogue structures with Pd and Pt,^[31–32] we started our investigations with it.

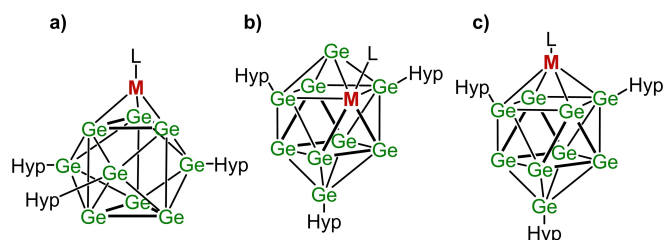


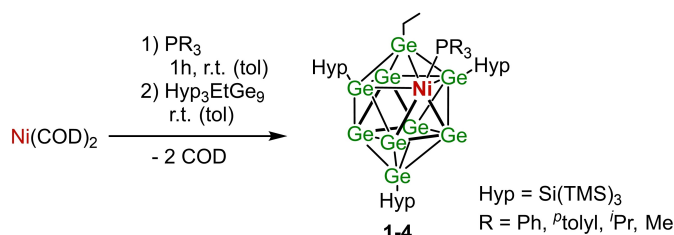
Figure 1. Schematic drawing of metalated cluster structures with a) the metal having an η^3 -coordination, b) the metal atom having η^2 -coordination, and c) the metal atom having η^4 -coordination. M stands for metal, and L stands for ligand.

Furthermore, as a benefit of nickel its abundance and, thus, lower costs make it attractive for catalytical applications. The species 1–4 were obtained by reacting $[\text{Hyp}_3\text{EtGe}_9]$ with an in situ generated “ NiPR_3 ” species in toluene (Scheme 1). Compounds 1, 3, and 4 could be crystallised from *n*-hexane solutions at -40°C , so single crystal X-ray diffraction was possible. In addition to the synthesis, their catalytic activity in olefin isomerisation was investigated.

Results and Discussion

Synthesis

Four compounds with ten-atomic $[\text{Ge}_9\text{Ni}]$ cores were synthesised through the reaction of $\text{Hyp}_3\text{EtGe}_9$ with $\text{Ni}(\text{COD})_2$ in the presence of the respective phosphines in toluene at room temperature. This reaction route does not require more sophisticated Ni complexes as they were used before, but commercially available $\text{Ni}(\text{COD})_2$. The products $\text{Hyp}_3\text{Et}[\text{Ge}_9\text{Ni}]\text{PR}_3$ ($R = \text{Ph}$, $^t\text{olyl}$, ^iPr and Me ; 1, 2, 3 and 4, respectively) were characterised *via* NMR spectroscopy, LIFDI/MS and elemental analysis. The new species 1–4 show identical or analogous NMR spectra to previously reported $\text{Hyp}_3\text{Et}[\text{Ge}_9\text{Ni}]\text{PPh}_3$ ^[32] (Figures S2–S8, S10–S15, S17–S27, S29–S33, Supporting Information). LIFDI/MS measurements (Figure S9, S16, S28, S34, Supporting Information) prove the successful synthesis of 1–4 through this easy synthetic approach. Compared to the reported reaction route for 1^[32] the yield has been raised from 27% to 67%. ^1H NMR spectra show two characteristic signal groups for the hypersilyl substituents, the signals for the ethyl group and the signals for the phosphine ligands. Remarkably compounds 1, 2 and 4 show broader signals for the TMS groups and the ethyl group than 3, which can be interpreted with the different steric demand of the phosphine ligands. P^iPr_3 has a significantly larger cone angle of 160° than that of the other ones (PPh_3 145° ; P^tolyl_3 145° ; PMe_3 115°), anticipating less dynamic behaviour at room temperature by sharp signals in the ^1H NMR spectrum.^[35] Furthermore, the signals for the hypersilyl and ethyl groups in 3 retain a narrow signal width over the whole temperature range between -90°C and 90°C (Figures S24 and S25, Supporting Information). So, the signal groups for the ethyl substituent can be clearly identified as a quartet and a triplet. In contrast, these are broad signals for species 1, 2 and 4. ^{31}P NMR spectra reveal a low field shift of the signals of 1–4 by 50 to 65 ppm compared



Scheme 1. Reaction of $[\text{Hyp}_3\text{EtGe}_9]$ with $\text{Ni}(\text{COD})_2$ and different phosphines PR_3 ($R = \text{Ph}$, $^t\text{olyl}$, ^iPr , Me) in toluene to yield $\text{Hyp}_3\text{Et}[\text{Ge}_9\text{Ni}]\text{PR}_3$ (1–4).

to the non-coordinated ligands. Interestingly, this is in contrast to known high-field shifts of metal-bound phosphine ligands since, in general, PR_3 groups act as electron donors to the metal atom.^[36–37] The low field shift here hints at a strong π -backdonation^[36–37] which can be rationalised that the Ge_9 clusters – despite their electron deficiency according to *Wade* rules – appear as electron donors for the Ni atoms. The magnitude of the shifts of the different phosphine ligands is in accordance with their steric demand according to the known fact that an increase in cone angle causes a stronger low field shift.^[35] Thus the most bulky ligand P^tPr_3 has a shift of around 84 ppm, followed by PPh_3 with 51 ppm, P^otolyl_3 with 49 ppm and PMe_3 with –13 ppm.

Single crystals of products $\text{Hyp}_3\text{Et}[\text{Ge}_9\text{Ni}]\text{P}^t\text{Pr}_3$ (**3**) and $\text{Hyp}_3\text{Et}[\text{Ge}_9\text{Ni}]\text{PMe}_3$ (**4**) were obtained through crystallisation from *n*-hexane at -40°C (Figure 2).^[38] Both cluster cores adopt a C_s -symmetric distorted bicapped square antiprism of $[\text{Ge}_9\text{Ni}]$, with an idealised mirror plane through the atoms Ni, Ge1, Ge3 and Ge9. Within these structures, the nickel atom represents a vertex of one square of the antiprism and is bound to five germanium atoms (Ge1, Ge2, Ge4, Ge5 and Ge6). Overall, five substituents are attached to the cluster core: Three hypersilyl groups bound to Ge2, Ge4 and Ge9, one ethyl group bound to Ge1 and the phosphine ligand bound to the nickel atom. This described structure of these clusters corresponds to the related literature known compounds $\text{Hyp}_3\text{Et}[\text{Ge}_9\text{M}]\text{PPh}_3$ ($\text{M}=\text{Ni}, \text{Pd}$,

Pt)^[31–32] and the attachment of different phosphine ligands does not influence the structure of the cluster. The Ge-Ge bond lengths within the cluster cores in **3** and **4** lie in the range of 2.4601(5)–2.8172(5) Å and 2.4886(6)–2.8186(7) Å, with Ge1-Ge2 being the shortest and Ge1-Ge3 being the longest distance. The bond lengths in species **3** and **4** are in good accordance with the literature known analogues MPPH_3 ($\text{M}=\text{Ni}, \text{Pd}, \text{Pt}$) with distances in the range of 2.4682(6)–2.8020(6) Å for Ni, 2.4548(7)–2.8283(7) Å for Pd, and 2.4756(8)–2.8885(9) Å for Pt.^[31–32] Furthermore, the Ni–P bond length in **4** of 2.159(1) Å is a bit shorter than the one reported for NiPPH_3 with 2.180(1) Å, which is due to the sterically less demanding phosphine ligand in **4**.^[32] Species **3**, including the phosphine with the largest ligand cone angle, possesses the longest Ni–P distance with 2.200(1) Å. In addition to the elongation of the Ni–P bond through increasing the steric demand on the nickel atom, the ethyl ligand bound to Ge1 shows a different orientation with respect to the phosphine ligand facing away from it. This has also been observed in known $\text{Hyp}_3\text{Et}[\text{Ge}_9\text{Ni}]\text{PPh}_3$.^[32] Since all Ge–Ni–P bonding angles lie in the same range of 111.88(3)–134.95(4)° for **3**, 108.69(4)–134.58(4)° for **4** and 112.29(3)–132.38(4)° for NiPPH_3 no influence of the steric demand of the ligand is present.^[32] Additionally, XPS measurements on **1–4** have been performed (Table S6 and Figures S38 and S39, Supporting Information). The resulting spectra are quite similar for all four compounds, and the regions of the binding energies

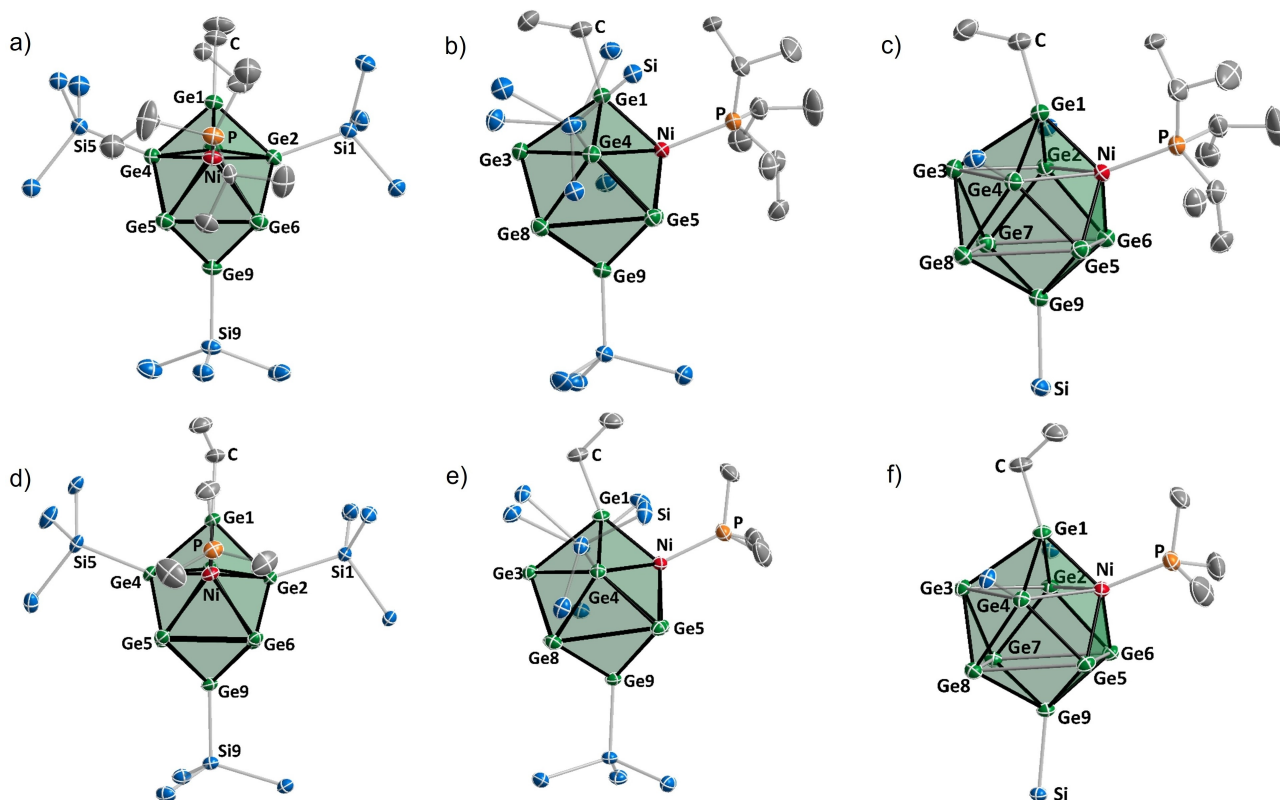


Figure 2. Three orientations of the molecular structures a)–c) $\text{Hyp}_3\text{Et}[\text{Ge}_9\text{Ni}]\text{P}^t\text{Pr}_3$ (**3**) and d)–f) $\text{Hyp}_3\text{Et}[\text{Ge}_9\text{Ni}]\text{PMe}_3$ (**4**).^[38] All displacement ellipsoids are shown at a probability level of 50%. The $[\text{Ge}_9\text{Ni}]$ cluster cores are depicted as green polyhedra. Ge, Si, Ni, P and C atoms are depicted in green, blue, red, orange, and grey colours, respectively. Methyl groups at the hypersilyl substituents and all hydrogen atoms are omitted for clarity. In figures c and f, only the silicon atoms directly bound to the cluster core are shown for simplicity.

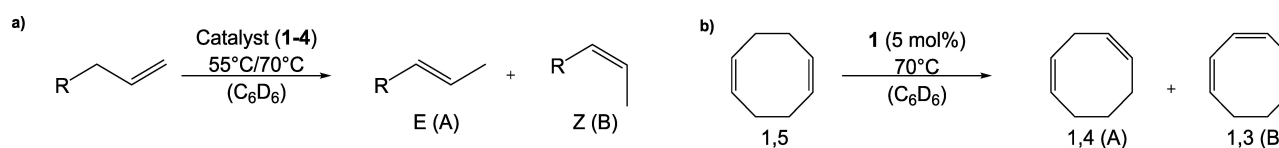
can be related to $\text{Ge}^{0\text{II}}$ species, Ni^0 and Si^{III} species. This underlines the comparison between our clusters and *single site* catalysts, whereby our metal atom has the oxidation state zero and is non-oxidised like in classical *SSHCS*.

Catalytic activity

The catalytic activity of compounds **1-4** was tested by means of olefin isomerisation reactions, which have also been reported for different Ni-complexes such as $\text{NiX}_2(\text{PPh}_3)_2$ ($\text{X} = \text{Cl, Br, I}$),^[39] β -diketiminato-nickel(II)bromide,^[40] $(^{\text{Ph}}\text{PSiP})\text{Ni}(\text{C}_8\text{H}_{13})$ ($^{\text{Ph}}\text{PSiP} = \text{Si}(\text{Me})(2\text{-PPh}_2\text{-C}_6\text{H}_4)_2$),^[41] and η^3 -allyl-nickel(II) complexes.^[42] Also, for the above-mentioned Ir-siliconoid species the possibility of such reactions with participating clusters was proven.^[34] Adding 1-hexene to a solution of $\text{Hyp}_3\text{Et}[\text{Ge}_3\text{Ni}]\text{PPh}_3$ in C_6D_6 , results in the isomerisation to 2-*E*- and 2-*Z*-hexene, which were identified by GC/MS and ^1H NMR spectroscopy (Scheme 2a, Table 1, entries 1–3). Figure 3a shows the course of isomerisation in the presence of 5 (blue squares) and 2 mol% of **1** at 70 °C (green triangles), respectively, and 5 mol% of **1** at 55 °C (orange triangles) monitored by ^1H NMR spectroscopy. 2-*Z*-hexene is the primary product of the isomerisation, whereas the amount of 2-*E*-hexene increases with time reaching an equilibrium at a ratio of 2-*E*-hexene:2-*Z*-hexene = 70:30 (5 mol%) and 60:40 (2 mol%) (Figure S40, Supporting Information). This indicates that 2-*Z*-hexene is converted to 2-*E*-hexene during the reaction, which

was independently shown by using 2-*Z*-hexene as the starting material, which gave the same final product ratio of 70:30 (Figure S43, Supporting Information). During the isomerisation reaction, free PPh_3 was formed, which was detected by ^{31}P NMR spectroscopy (Figure S42, Supporting Information). In addition, the isomerisation rate was lower in the presence of 15 mol% PPh_3 based on the amount of 1-hexene compared to the reaction mixture without further addition of a phosphine (Figure 3a) which hints for $\text{Hyp}_3\text{Et}[\text{Ge}_3\text{Ni}]$ with dissociated phosphine ligand is the catalytically active species. Compounds **2**, **3** and **4** were tested as catalysts (5 mol% at 70 °C; Table 1 entries 4–6). The catalytic activity of **2** was similar to **1**, compound **3** was significantly less active, and **4** showed very low activity in the isomerisation reaction of 1-hexene (Figure 3b). Nevertheless, in all cases, 2-*E*- and 2-*Z*-hexene are exclusively formed as isomerisation products with higher amounts of the *E*-isomer reaching an equilibrium in the range of *E*:*Z* = 60:40 to 70:30, according to the NMR and GC/MS results (Figures S44–S49, Supporting Information). Whereas the uncoordinated phosphine ligand was detected during the reaction with compounds **2** and **3**, with **4**, no free PMe_3 was found. These observations underline the necessity to cleave off the phosphine ligand from the nickel atom so that a free binding site is generated, making catalysis possible.

Furthermore, it was shown that **1** analogously isomerises allylcyclohexane and allylbenzene under the conditions applied for 1-hexene (5 mol% **1** at 70 °C, Figure 3a, Table 1 entries 7 and



Scheme 2. Products of the isomerisation reaction of a) 1-hexene, allylcyclohexane and allylbenzene in the presence of **1-4** and b) COD with **1** in C_6D_6 . ($\text{R} = \text{C}_3\text{H}_7$, cyclohexyl, phenyl).

Table 1. Isomerisation of different olefins (0.229 mmol) in the presence of **1-4** in 0.5 mL benzene- d_6 and performed blank tests for the isomerisation of 1-hexene.

Entry	Olefin	Compound	T [°C]/t [h]	Conversion [%]	(A/B) ^[a] /(A/B) ^[b]
1	1-hexene	1 (5 mol%)	70/55.5	95	(70/30)/(76/24)
2	1-hexene	1 (5 mol%)	55/95	95	(70/30)/(75/25)
3	1-hexene	1 (2 mol%)	70/197	89	(60/40)/(58/42)
4	1-hexene	2 (5 mol%)	70/44	92	(61/39)/(60/40)
5	1-hexene	3 (5 mol%)	70/487	84	(67/33)/(70/30)
6	1-hexene	4 (5 mol%)	70/265	11	(53/47)/(53/47)
7	allylcyclohexane	1 (5 mol%)	70/449	66	-(45/55)
8	allylbenzene	1 (5 mol%)	70/189	93	(90/10)/(91/9)
9	COD	1 (5 mol%)	70/142	70	(31/69)/(30/70)
10	1-hexene	$[\text{Hyp}_3\text{EtGe}_3]$ (5 mol%)	70/208	0	-/-
11	1-hexene	$\text{Ni}(\text{COD})_2 + \text{PPh}_3$ (5 mol%)	70/80	2	(46/53)/-
12	1-hexene	$\text{Ni}(\text{PPh}_3)_4$ (5 mol%)	70/74	4	(40/60)/-
13	1-hexene	PPh_3 (5 mol%)	70/74	0	-/-

[a] According to ^1H NMR. [b] According to GC/MS.

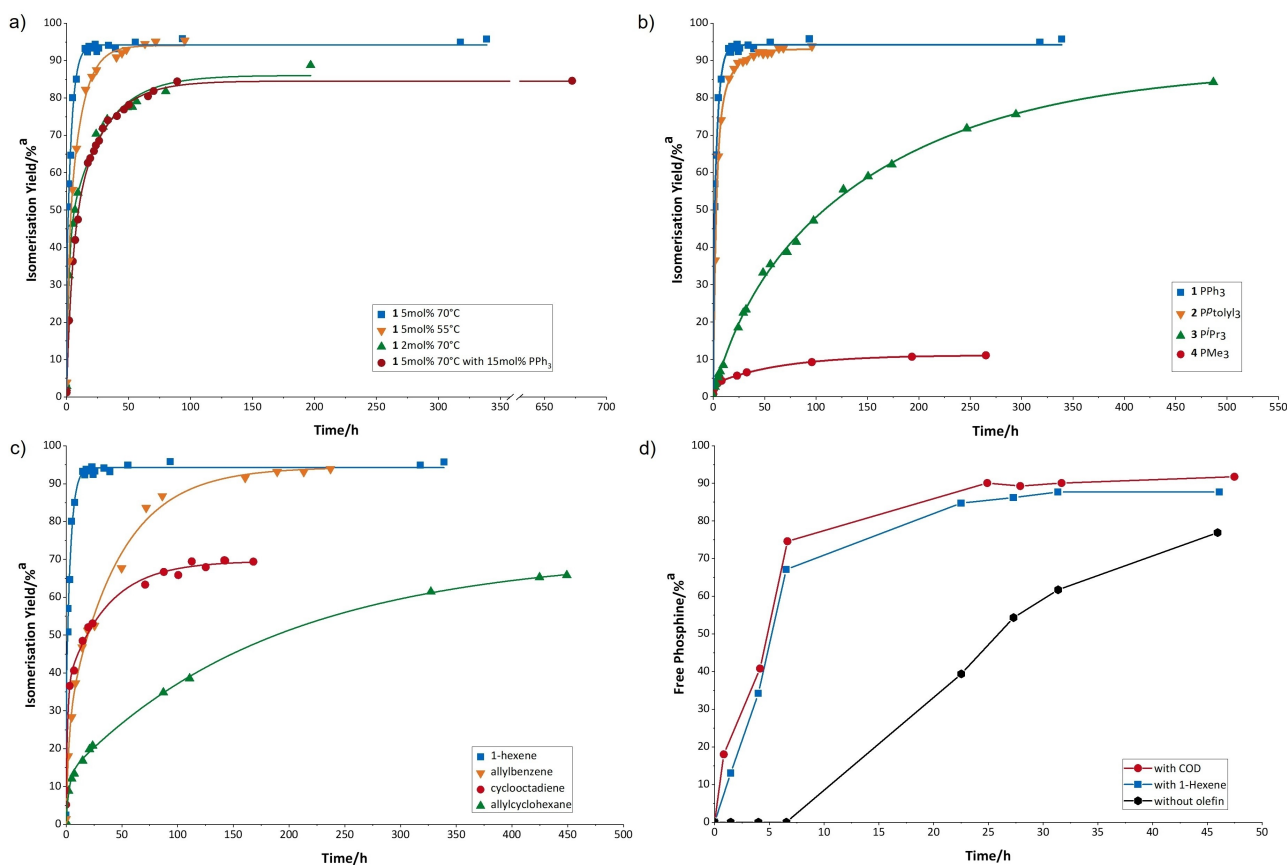


Figure 3. Kinetic measurements of a) the isomerisation of 1-hexene in the presence of **1** under various conditions (5 mol% **1** at 70 °C (blue squares), 5 mol% **1** at 55 °C (orange triangles), 2 mol% **1** at 70 °C (green triangles) and 5 mol% **1** at 70 °C in the presence of 15 mol% PPh₃ (red dots)); b) the isomerisation of 1-hexene with **1** (blue squares), **2** (orange triangles), **3** (green triangles) and **4** (red dots) at 70 °C with 5 mol% cluster; c) the isomerisation of 1-hexene (blue squares), allylbenzene (orange triangles), COD (red dots) and allylcyclohexane (green triangles) with **1** at 70 °C with 5 mol% cluster; d) the dissociation of the phosphine ligand of **1** over time at 70 °C (red dots with 70 equiv. of COD, blue squares with 70 equiv. of 1-hexene and black hexagons without the addition of olefin). All experiments were performed in C₆D₆. ^aAccording to NMR standard procedure in an NMR tube and measured using ¹H NMR or ³¹P NMR.

8, Figures S50–S53, Supporting Information). The isomerisation rate decreases thereby in the order: 1-hexene > allylbenzene > allylcyclohexane probably due to the increased steric demand of the residues. However, it is noticeable that the E-isomer is more favoured for allylbenzene. For COD both possible isomerisation products, cycloocta-1,4-diene and cycloocta-1,3-diene (Figure 3b, Table 1 entry 9), were detected using NMR and GC/MS analysis (Figures S54 and S55, Supporting Information). All applied reactions underline the catalytic potential of Ni-metalated *Zintl* clusters since we can affirm that no traces of Ni-precursors, pure Ni metal or the cluster precursor [Hyp₃EtGe₉] are responsible for the catalysis. Even the pure phosphine ligands or mixtures of phosphine and Ni(COD)₂ are catalytically inactive (Table 1 entries 10–13). As mentioned above, isomerisation reactions have also been reported for the Ni-complexes β-diketiminato-nickel(II)bromide,^[40] (P^hPSiP)Ni(C₈H₁₃),^[41] and η³-allyl-nickel(II) complexes^[42] as well as for the Ir-siliconoid.^[34] In order to obtain a catalytic species in the case of β-diketiminato-nickel(II)bromide and (P^hPSiP)Ni(C₈H₁₃), nickel-hydride species are generated through methylation with methylaluminiumoxane (MAO)^[40] and through β-hydride elimination of the coordinated C₈H₁₃,^[41] respectively. Also, for the η³-allyl-

nickel(II) complexes, special activation by adding B(C₆F₅)₃ is required.^[42] In contrast, clusters 1–4 also reach conversions up to 95% (for **1**) solely by ligand cleavage without any special activation processes. Hereby the phosphine ligand can be replaced by toluene or benzene in solution, which can be further substituted by the substrate. Since the solvent and the substrates are present in excess, the equilibrium of these processes is shifted towards the phosphine free species (Figure 4). The Ir-siliconoid, on the other hand, does not require any activation step or ligand cleavage since the COD ligand can tilt away for the generation of a vacant binding side. With this Ir-species, even at r.t., conversions up to 97% in the isomerisation of 1-hexene are possible at very low catalyst loadings of 0.05–0.1 mol% at r.t., while for bulkier substrates higher temperatures of 60 °C are necessary.^[34] Considering all these aspects, the [Ge₉Ni] cluster, which uses a more abundant and cheaper metal for catalysis, can definitely compete with such systems.

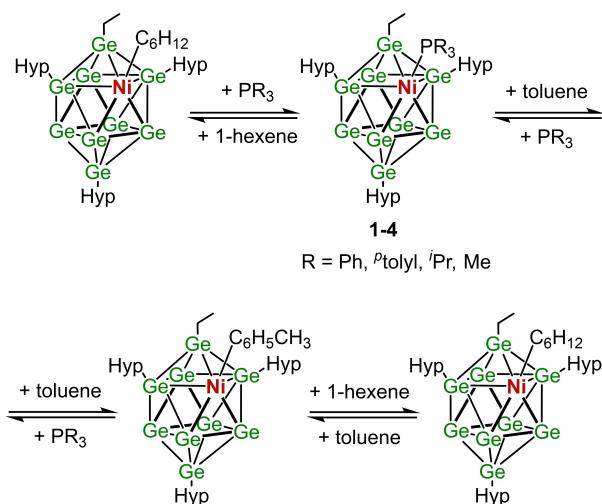


Figure 4. Exchange reactions between the phosphine ligands and the solvent (toluene or benzene) or/and the substrate 1-hexene. All processes are equilibrium reactions.

Formation of an active Ni site

Since we observed free phosphine during the isomerisation reactions, we studied the ligand cleavage in the absence of an olefin. An earlier report on $\text{Hyp}_3\text{Et}[\text{Ge}_9\text{Ni}]\text{PPh}_3$ showed that phosphine cleavage was observed upon heating, although the amounts of free PPh_3 were very small.^[32] We verified by variable temperature ^{31}P NMR spectroscopy of **1** between 0°C and 90°C (Figure S7, Supporting Information) that actually ligand cleavage occurs at higher temperatures. At 70°C , free ligand dissociation appeared after six hours in amounts that were detectable by ^{31}P NMR measurements, and the percentage of cleaved PPh_3 grew within 47 hours up to 77% (Figure 3d, black hexagons). Since ligand cleavage seemed to occur faster in the isomerisation reactions, we added an excess of 1-hexene or COD to a solution of **1** in C_6D_6 and monitored again the phosphine cleavage over time. As shown by blue squares and red dots in Figure 3d, respectively, the ligand cleavage occurs immediately at 70°C and proceeds faster. In the presence of 1-hexene, 33% and 88% of free PPh_3 are detected after 90 minutes and 46 hours, respectively. COD is even more effective, with 18% after one hour and 94% after 47.5 hours. This indicates, that the replacement of the phosphine ligand by olefins is favoured towards substitution by the aromatic solvent (Figure 4). Since catalysis with P^ntolyl_3 works almost as well as with PPh_3 , it can be assumed that the cleavability of the phosphine ligand in solution without olefin is similar to PPh_3 . In contrast, $\text{Hyp}_3\text{Et}[\text{Ge}_9\text{Ni}]\text{P}^i\text{Pr}_3$ (**3**) shows less catalytic activity, with less detectable dissociation under equivalent conditions. In the variable temperature ^1H and ^{31}P NMR spectra in the range from -90°C to 90°C (Figures S23 and S26, Supporting Information), the only visible signals arise from P^iPr_3 that binds to the nickel atom. Signals of free P^iPr_3 that had been observed during the catalytic isomerisation reaction were not observed also at higher temperatures. Also, for $\text{Hyp}_3\text{Et}[\text{Ge}_9\text{Ni}]\text{PMe}_3$ (**4**), which shows the least catalytic activity, no free phosphine during the

catalysis could be detected. The results indicate that not only the steric demand but most probably also the electronic effect of the phosphine ligand seems to be an important factor for the dissociation process. During attempts to replace PPh_3 in **1** by P^iPr_3 we observed PPh_3 cleavage at elevated temperatures and formation of $\text{Hyp}_3\text{Et}[\text{Ge}_9\text{Ni}]\text{P}^i\text{Pr}_3$ in however very small amounts as indicated by a ^{31}P -NMR signal at 84.38 ppm (Figure S56, Supporting Information). Cooling the mixture for several hours to -32°C preferably leads again to the formation of **1**.

Computational study

DFT calculations have been performed in order to gain additional insight into the thermal behaviour and the catalytic activity of the $\text{Hyp}_3\text{Et}[\text{Ge}_9\text{Ni}]\text{PR}_3$ (R = Ph, ⁿtolyl, ⁱPr, Me) clusters in solution. The standard Gibbs free energy, ΔG_1° , for phosphine dissociation from the nickel atom, i.e. $\text{Hyp}_3\text{Et}[\eta^5\text{-Ge}_9\text{Ni}]\text{PR}_3 \rightarrow \text{Hyp}_3\text{Et}[\eta^5\text{-Ge}_9\text{Ni}] + \text{PR}_3$ (Figure 4 and Figure 6), was calculated to 36.2 (R = Me), 35.9 (R = Ph) and 24.6 $\text{kcal}\cdot\text{mol}^{-1}$ (R = ⁱPr), respectively. These rather high values preclude a simple phosphine dissociation in solution. Thus, in order to explain the observed behaviour at elevated temperatures in a toluene or benzene solution, displacement of the phosphine ligand by the solvent was considered. And, indeed, the standard Gibbs free energies for such a reaction were found to be lower ($\text{Hyp}_3\text{Et}[\eta^5\text{-Ge}_9\text{Ni}]\text{PR}_3 + \text{C}_6\text{H}_5\text{CH}_3 \rightarrow \text{Hyp}_3\text{Et}[\eta^5\text{-Ge}_9\text{Ni}](\eta^2\text{-C}_6\text{H}_5\text{CH}_3) + \text{PR}_3$, $\Delta G_2^\circ = 24.4$ (R = Me), 24.1 (R = Ph) and 11.7 $\text{kcal}\cdot\text{mol}^{-1}$ (R = ⁱPr), Figure 4 and Figure 6). Considering the elevated temperatures and the large excess of toluene or benzene in the reaction mixture, formation of $\text{Hyp}_3\text{Et}[\eta^5\text{-Ge}_9\text{Ni}](\eta^2\text{-C}_6\text{H}_5\text{CH}_3)$ in an equilibrium might be plausible. Surprisingly, the values of ΔG_1° and ΔG_2° are lowest for R = ⁱPr, indicating that this ligand is bound the weakest among the investigated phosphines. Since no ligand displacement was observed for R = ⁱPr but for the thermodynamically more strongly bound PPh_3 , kinetic reasons must be considered. A tentative mechanism might involve the initial coordination of toluene/benzene to the nickel center of the phosphine complexes followed by dissociation of the phosphine. Looking at a space-filling model of the phosphine complexes (Figure 5), it is obvious that the nickel center is most shielded in $\text{Hyp}_3\text{Et}[\eta^5\text{-Ge}_9\text{Ni}]\text{P}^i\text{Pr}_3$, indicating that this complex is meta-stable/inert toward ligand displacement.

In the catalytic isomerisation of olefins, a similar mechanism might be operative as indicated by calculations using 1-hexene as a model substrate. Here, the standard Gibbs free energies for the displacement of a phosphine ligand by 1-hexene ($\text{Hyp}_3\text{Et}[\eta^5\text{-Ge}_9\text{Ni}]\text{PR}_3 + \text{C}_6\text{H}_{12} \rightarrow \text{Hyp}_3\text{Et}[\eta^5\text{-Ge}_9\text{Ni}](\eta^2\text{-C}_6\text{H}_{12}) + \text{PR}_3$, $G = 15.9$ (R = Me), 15.6 (R = Ph) and 10.6 $\text{kcal}\cdot\text{mol}^{-1}$ (R = ⁱPr), Figure 4 and Figure 6), are even lower compared to displacement of a phosphine ligand by toluene (vide supra). Thus, at elevated temperatures and at high excess of the substrate, facile displacement might occur. These rather low Gibbs free reaction energies might be explained by the conformation of alkyl/silyl substituents at the Ge_9 cluster, which offer a suitable binding pocket for 1-hexene.

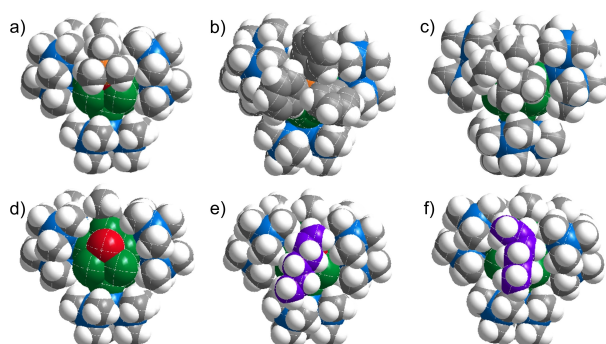


Figure 5. Space filling models of a) $\text{Hyp}_3\text{Et}[\text{Ge}_9\text{Ni}]\text{PMe}_3$, b) $\text{Hyp}_3\text{Et}[\text{Ge}_9\text{Ni}]\text{PPh}_3$,^[32] c) $\text{Hyp}_3\text{Et}[\text{Ge}_9\text{Ni}]\text{P}^i\text{Pr}_3$ d) $\text{Hyp}_3\text{Et}[\text{Ge}_9\text{Ni}]\text{CH}_2\text{CH}(\text{CH}_2)_3\text{CH}_3$ and f) $\text{Hyp}_3\text{Et}[\text{Ge}_9\text{Ni}]\text{CH}_3(\text{CH}_2)_2\text{CH}_3$. Ge, Si, Ni, P, C and H atoms are depicted in green, blue, red, orange, grey and white colour, respectively. For better visualisation, the carbon atoms of the hexene molecules are depicted in purple.

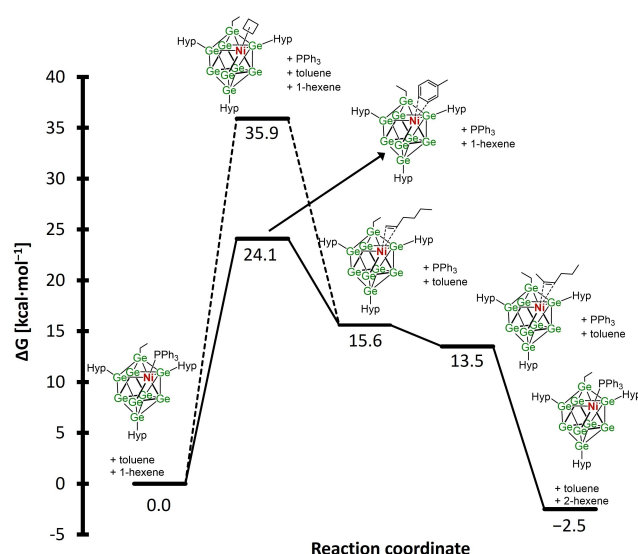


Figure 6. Calculated ΔG values for the isomerisation of 1-hexene to 2-hexene with **1**.

Subsequently, isomerisation of 1-hexene to 2-Z-hexene at the nickel centre occurs in an almost thermoneutral reaction ($\Delta G_3^\circ = -2.1 \text{ kcal}\cdot\text{mol}^{-1}$). Finally, 2-hexene is replaced by 1-hexene closing the catalytic cycle ($\Delta G_4^\circ = 2.1 \text{ kcal}\cdot\text{mol}^{-1}$). The observed higher catalytic activity of PPh_3 compared to P^iPr_3 , despite the latter being bound weaker, could again hint at a two-step displacement mechanism for the reaction, where first the coordination of the substrate at nickel is necessary to facilitate phosphine displacement. Calculations of the binding energies show, that PPh_3 and PMe_3 are almost bounded with equal strength, followed by P^iPr_3 , which has the weakest bond to nickel (Table S24, Supporting Information). To explain the catalytic activities, however, also steric effects and Ni–P bond lengths are considered. The steric shielding offered by the P^iPr_3 ligand might prevent the substrate from reaching the nickel atom even the P^iPr_3 derivative has the longest Ni–P bond of $2.200(1) \text{ \AA}$, explaining the lower catalytic activity of $\text{Hyp}_3\text{Et}[\eta^5\text{-Ge}_9\text{Ni}]\text{P}^i\text{Pr}_3$. Even though, PMe_3 and PPh_3 possess almost the

same binding energies, they differ in their catalytic activity. This can be explained by the shorter Ni–P bond length in $\text{Hyp}_3\text{Et}[\eta^5\text{-Ge}_9\text{Ni}]\text{PMe}_3$ of $2.159(1) \text{ \AA}$ compared to $2.180(1) \text{ \AA}$ for the PPh_3 derivative,^[32] that more effectively shields the Ni atom, preventing attachment of the substrate molecule which is necessary for the associative mechanism. For PPh_3 the situation seems to be optimal concerning its steric demand and bond length.

Conclusions

XPS measurements reveal that in $\text{Hyp}_3\text{Et}[\text{Ge}_9\text{Ni}]\text{PPh}_3$ a single Ni^0 atom is embedded in a Ge environment with mainly Ge^0 atoms. Due to the newly developed straightforward synthetic route, the phosphine ligands at the nickel atom could be varied and $\text{Hyp}_3\text{Et}[\text{Ge}_9\text{Ni}]\text{PR}_3$ ($\text{R} = \text{Ph}_3$, **1**; $^p\text{tolyl}$, **2**; ^iPr , **3** and Me , **4**) were obtained in good quantities. The catalytic ability of **1–4** in the isomerisation of 1-hexene decreases in the order $\text{PPh}_3 \approx \text{P}^p\text{tolyl}_3 > \text{P}^i\text{Pr}_3 > \text{PMe}_3$. It is shown that phosphine ligand dissociation is crucial for the catalytic activity and even the isomerisation of sterically more demanding olefins with **1** as catalyst were successful. Since in all isomerisation reactions, the cleavage of the ligand was detected, $\text{Hyp}_3\text{Et}[\text{Ge}_9\text{Ni}]$ with a free coordination site at the Ni atom must be considered as the active species. DFT calculations show that the free metal atom site is stabilized by the intermediate coordination of solvent molecules.

Thus, for the first time it is shown that a single metal atom with oxidation state 0 and with a free binding site is stabilized at the surface of a small, soluble germanium atom cluster. Single metal atom sites have been produced in so-called single site catalysts in heterogeneous catalysis and this is now introduced for soluble, homogeneous catalysts. In contrast to single site heterogeneous catalysts, in which single site metal atoms may agglomerate and for which atom leakage cannot be excluded, the metal atom in the here reported homogeneous single site catalysts binds strongly to the Ge cluster atoms and remains attached even when protecting ligands are removed. This leads to outstanding catalytic properties. Here we have shown, that the less noble Ni^0 atom remains stable and shows catalytic properties while the Ge cluster itself is not directly involved in the catalytic reaction and can be regarded as innocent.

Experimental Section

General

All manipulations were performed under a purified argon atmosphere using standard Schlenk and glovebox techniques. The solvents acetonitrile, toluene and hexane were dried over molecular sieves using the solvent purification system MB-SPS. All deuterated solvents were purchased from *Sigma-Aldrich* and stored over molecular sieves (3 \AA). The *Zintl* Phase with nominal composition K_4Ge_9 was synthesised by heating a stoichiometric mixture of the elements K (*Merck* 99.8%) and Ge (*Chempur*, 99.999%) at 650°C for 46 h in a stainless steel autoclave.^[12] Hypersilylchloride (*Sigma-*

Aldrich, 97%), ethylbromide (*Sigma-Aldrich*, $\geq 99\%$), triphenylphosphine (*Merck*, $> 98\%$), triisopropylphosphine (*Acros Organics*, 98%), triparatolylphosphine (*Sigma-Aldrich*, 98%), trimethylphosphine (*Sigma-Aldrich*, 1.0 M in toluene), bis(cyclooctadiene)nickel(0) (*Sigma-Aldrich*), 1-hexene (*Sigma-Aldrich*, $\geq 99\%$), 2-Z-hexene (*Sigma-Aldrich*, 95%), allylbenzene (*Sigma-Aldrich*, 98%), allylcyclohexane (*Sigma-Aldrich*, 96%) and cycloocta-1,5-diene (*Sigma-Aldrich*, 99%) were used as received.

NMR spectroscopy

All NMR spectra were recorded on a *Bruker Avance Ultrashield* 400 MHz or a *Bruker Avance Ultrashield* 500 MHz Cryo system spectrometer. The signals of ^1H and ^{13}C spectra were referenced to the signals of the used deuterated solvents C_6D_6 (7.16 ppm; 128.06 ppm) and toluene- d_8 (2.08 ppm, 6.97 ppm, 7.01 ppm, 7.09 ppm; 137.48 ppm, 128.87 ppm, 127.96 ppm, 125.13 ppm, 20.43 ppm).^[43] Chemical shifts are given in δ values in parts per million (ppm). The coupling constants J are stated in Hz. Signal multiplicities are abbreviated as follows: s – singlet, dd – doublet of doublet, t – triplet, q – quartet, h – septet, m – multiplet, and br – broad signal. Variable temperature NMR studies were performed on a *Bruker Avance Ultrashield* 400 MHz for ^1H and $^{31}\text{P}\{^1\text{H}\}$. The spectra were evaluated with the program *MestReNova*.^[44]

Elemental analysis

Elemental analysis was performed by the microanalytical laboratory at the Catalytic Research Centre of the Technical University of Munich. The elements C and H were determined by a combustion analyser (elementar vario EL, *Bruker Corp.*). Nickel was determined by atomic absorption spectroscopy.

Single crystal structure determination

For single crystal data collection, a few crystals were transferred from the mother liquor into perfluoropolyalkylether under a cold N_2 gas stream. A single crystal was fixed on a glass fibre and positioned in a 150 K cold N_2 gas stream. Single crystal data collection was performed with a *STOE StadiVari* (Mo $K\alpha$ radiation) diffractometer equipped with a *DECTRIS Pilatus* 300 K detector by using the X-Area software package.^[45] The crystal structures were solved by Direct Methods using *SHELX* software.^[46–47] The positions of the hydrogen atoms were calculated and refined using a riding model. Unless otherwise stated, all non-hydrogen atoms were treated with anisotropic displacement parameters. For compound **3** the atoms of the P^iPr_3 as well as one of the Hyp groups had to be refined at two split positions leading to site occupations of 85:15 and 93:7, respectively, and some of the minor occupied C atoms were refined isotropically. Both the compounds **3** and **4** crystallize with one molecule hexane per formula unit, which are disordered and, thus, their electron density was treated with the Platon Squeeze option.^[48] For visualisation, the crystal structures have been plotted with *Diamond*.^[49]

DFT calculations

All calculations were carried out with the ORCA program package.^[50–51] Unless stated otherwise, all calculations were carried out on isolated molecules (in the gas phase). Density fitting techniques, also called resolution-of-identity approximation (RI),^[52] were used for *meta*-GGA calculations. Atom-pairwise dispersion corrections (D3BJ or D4)^[53–55] were used for all DFT calculations. All geometries, thermal and entropic corrections were obtained at the

BP86-D3BJ/def2-SVP^[56] level of theory. Subsequently, electronic energies were obtained using TPSS–D4/def2-TZVPP.^[56–57]

GC/MS

GC/MS analysis was performed on an *Agilent Technologies GC7890B* with HP-5MS UI column (length 30 m, internal diameter 0.25 mm, film 0.25 μm) equipped with an MS 5977 A with a single quadrupole mass detector. Standard method used for separation of compounds 35 °C [1 min], 15 °C/min \rightarrow 270 °C, 270 °C [5 min]. All substrates were clearly assigned by their mass or by comparison with authentic samples.

LIFDI/MS

Liquid Injection Field Desorption Ionization Mass Spectrometry (LIFDI/MS) was measured directly from an inert atmosphere glovebox with a *Thermo Fisher Scientific Exactive Plus Orbitrap* equipped with an ion source from Linden CMS.^[58]

X-Ray photoelectron spectroscopy

To investigate the near-surface chemical state X-ray photoelectron spectroscopy (XPS) was performed using an Axis Supra System (*Kratos*, UK). Therefore, the powders were pressed onto a stainless-steel stub inside an argon-filled glovebox and transported into the XPS without exposure to air. Throughout the entire measurement, the pressure was kept below $\sim 10^{-8}$ Torr. All samples were irradiated using monochromatic Al $K\alpha$ radiation (1486.6 eV) and an emission current of 15 mA. The survey scans were recorded from 1200 to -5 eV binding energy, using a step size of 0.5 eV and two sweeps. The Ni2p, Ni3p, Ge2p, Ge3p and Si2p regions were measured between 890–845 eV, 80–55 eV, 1230–1205 eV, 135–110 eV and 110–92 eV binding energy, using steps sizes of 0.1 eV and five sweeps. The samples were analysed without sputter cleaning, and the binding energies were corrected to the adventitious carbon peak at 284.8 eV. Data treatment was carried out using the program *CasaXPS* with application of a Shirley background.^[59]

Synthesis of [$\text{Hyp}_3\text{EtGe}_3$]

The compound [$\text{Hyp}_3\text{EtGe}_3$] was synthesised according to literature procedure.^[18] K_4Ge_9 (4.00 g, 4.9 mmol) and hypersilylchloride (4.19 g, 14.8 mmol) were weighed out into a Schlenk tube, and 25 mL acetonitrile were added. The resulting brown suspension is stirred for 6 h at r.t. and filtered over a glass fibre filter. Bromoethane (1.82 mL, 24.5 mmol) dissolved in 5 mL acetonitrile is added to the reaction mixture. The solution is stirred over night at r.t. while a brown precipitate is formed. The precipitate is separated from the solution by *Whatman* filtration, washed with 3x5 mL acetonitrile and dried *in vacuo*. Subsequently, it is redissolved in toluene and filtered again to remove any remaining solid. The resulting reddish solution is evaporated, and the product is characterised by NMR spectroscopy (Supporting Information Figure S1).

^1H NMR (400 MHz, C_6D_6 , 298 K): 0.41 (s, 81H, TMS), 1.47 (t, $^3J = 7.7$ Hz, 3H, CH_2CH_3), 1.81 (q, $^3J = 7.7$ Hz, 2H, CH_2CH_3).

Synthesis of $\text{Hyp}_3\text{Et}[\text{Ge}_9\text{Ni}]\text{PPh}_3$ (1)

$\text{Ni}(\text{COD})_2$ (193 mg, 0.7 mmol) and triphenylphosphine (182 mg, 0.7 mmol) were weighed into a Schlenk tube, and 7 mL toluene were added. The resulting dark red solution was stirred at r.t. for

one hour. This solution was added to a solution of [Hyp₃EtGe₃] (500 mg, 0.35 mmol) in 7 mL toluene. The brown reaction mixture was stirred at r.t. for 72 h. After filtration, the solvent was removed *in vacuo*, and the residue was washed with acetonitrile (3×5 mL). After drying in high vacuum, 406 mg of **1** (67%) were obtained as a brown solid. For crystallisation, a hexane solution of **1** was stored at −40 °C. Brown block-shaped crystals suitable for single crystal X-ray diffraction were obtained after 3 months. The crystal structure determination confirmed the result which was previously obtained by an alternative synthesis route.^[32]

¹H NMR (400 MHz, C₆D₆, 298 K): 0.30 (s, 54H, TMS), 0.64 (s, 27H, TMS), 2.28 (br, 3H, CH₂CH₃), 2.89 (br, 2H, CH₂CH₃), 6.96–7.05 (m, 3H, *p*-CH^{Ar}), 7.07–7.13 (m, 6H, *m*-CH^{Ar}), 7.75–7.80 (m, 6H, *o*-CH^{Ar}). ¹³C{¹H} NMR (100 MHz, C₆D₆, 298 K) 3.06 (TMS), 3.29 (TMS), 16.42 (CH₂CH₃), 37.86 (CH₂CH₃), 129.46 (m/*p*-CH^{Ar}), 134.33 (*o*-CH^{Ar}). ³¹P{¹H} NMR (162 MHz, C₆D₆, 298 K): 51.19 (PPh₃@Ni). LIFDI/MS: *m/z* = 1746.65 [Hyp₃EtGe₃NiPPh₃]⁺, 1484.36 [Hyp₃EtGe₃Ni]⁺. Elemental analysis calc.: C 32.32, H 5.83, Ni 3.36; found: C 32.40, H 5.91, Ni 3.38.

Synthesis of Hyp₃Et[Ge₃Ni]P^toly₃ (**2**)

Ni(COD)₂ (96.5 mg, 0.35 mmol) and triparatolyphosphine (106.7 mg, 0.35 mmol) were weighed into a Schlenk tube, and 5 mL toluene were added. The resulting dark red solution was stirred at r.t. for one hour. This solution was added to a solution of [Hyp₃EtGe₃] (250 mg, 0.17 mmol) in 5 mL toluene. The brown reaction mixture was stirred at r.t. for 72 h. After filtration, the solvent was removed *in vacuo*, and the residue was washed with acetonitrile (3×5 mL). After drying in high vacuum, 233 mg of **2** (77%) were obtained as a brown solid.

¹H NMR (400 MHz, C₆D₆, 298 K): 0.33 (s, 54H, TMS), 0.64 (s, 27H, TMS), 2.03 (s, 9H, ^{Ar}CH₃), 2.31 (br, 3H, CH₂CH₃), 2.93 (br, 2H, CH₂CH₃), 6.99–7.01 (m, 6H, *m*-CH^{Ar}), 7.74–7.79 (m, 6H, *o*-CH^{Ar}). ¹³C{¹H} NMR (100 MHz, C₆D₆, 298 K) 3.06 (TMS), 3.31 (TMS), 16.56 (CH₂CH₃), 21.14 (^{Ar}CH₃), 129.02 (*m*-CH^{Ar}), 134.16 (*o*-CH^{Ar}), 134.44 (*m*-CH^{Ar}). ³¹P{¹H} NMR (162 MHz, C₆D₆, 298 K): 48.81 (P^toly₃@Ni). LIFDI/MS: *m/z* = 1788.73 [Hyp₃EtGe₃NiP^toly₃]⁺, 1759.67 [Hyp₃Ge₃NiP^toly₃]⁺, 1541.07 [Hyp₂EtGe₃NiP^toly₃]⁺, 1484.36 [Hyp₃EtGe₃Ni]⁺, 1455.30 [Hyp₃Ge₃Ni]⁺, 1425.67 [Hyp₃EtGe₃]⁺.

Synthesis of Hyp₃Et[Ge₃Ni]PⁱPr₃ (**3**)

Ni(COD)₂ (96.5 mg, 0.35 mmol) and triisopropylphosphine (66.8 mg, 0.35 mmol) were weighed into a Schlenk tube, and 5 mL toluene were added. The resulting orange solution was stirred at r.t. for one hour. This solution was added to a solution of [Hyp₃EtGe₃] (250 mg, 0.17 mmol) in 5 mL toluene. The brown reaction mixture was stirred at r.t. for 72 h. After filtration, the solvent was removed *in vacuo*, and the residue was washed with acetonitrile (3×5 mL). After drying in high vacuum, 202 mg of **3** (72%) were obtained as a brown solid. For crystallisation, a hexane solution of **3** was stored at −40 °C. Brown block-shaped crystals suitable for single crystal X-ray diffraction were obtained after 3 months.

¹H NMR (400 MHz, toluene-*d*₈, 298 K): 0.32 (s, 54H, TMS), 0.65 (s, 27H, TMS), 1.11 (dd, ³J = 7.1 Hz, 18H, CH(CH₃)₂), 1.76 (h, ³J = 7.1 Hz, 3H, CH(CH₃)₂), 2.07 (t, ³J = 7.9 Hz, 3H, CH₂CH₃), 2.72 (q, ³J = 7.9 Hz, 2H, CH₂CH₃). ¹³C{¹H} NMR (100 MHz, toluene-*d*₈, 298 K) 3.38 (TMS), 3.84 (TMS), 16.97 (CH₂CH₃), 22.06 (CH(CH₃)₂), 26.46 (CH(CH₃)₂), 37.84 (CH₂CH₃). ³¹P{¹H} NMR (162 MHz, toluene-*d*₈, 298 K): 84.38 (PⁱPr₃@Ni). ²⁹Si{¹H} NMR (100 MHz, toluene-*d*₈, 298 K): −98.12 (Si(TMS)₃), −87.84 (Si(TMS)₂), −9.68 (SiMe₃), −8.72 (SiMe₃). LIFDI/MS: *m/z* = 1644.60 [Hyp₃EtGe₃NiPⁱPr₃]⁺, 1615.54 [Hyp₃Ge₃NiPⁱPr₃]⁺, 1484.36 [Hyp₃EtGe₃Ni]⁺, 1455.30 [Hyp₃Ge₃Ni]⁺, 1425.67 [Hyp₃EtGe₃]⁺, 1396.95 [Hyp₂EtGe₃NiPⁱPr₃]⁺, 1236.71 [Hyp₂EtGe₃Ni]⁺, 1178.02

Table 2. Performed isomerisation reactions.^aWith the addition of 15 mol% PPh₃.

Olefin	Catalyst (mol%)	T [°C]/t [h]
1-hexene	1 (5)	70/55.5
1-hexene	1 (5)	55/95
1-hexene	1 (2)	70/197
2-Z-hexene	1 (5)	70/221
1-hexene ^b	1 (5)	70/672
1-hexene	2 (5)	70/44
1-hexene	3 (5)	70/487
1-hexene	4 (5)	70/265
allylcyclohexane	1 (5)	70/449
allylbenzene	1 (5)	70/189
cycloocta-1,5-diene (COD)	1 (5)	70/168

[Hyp₂EtGe₃]⁺. Elemental analysis calc: C 27.75, H 6.56, Ni 3.57; found: C 26.64, H 6.25, Ni 3.54.

Synthesis of Hyp₃Et[Ge₃Ni]PMe₃ (**4**)

Ni(COD)₂ (96.5 mg, 0.35 mmol) and trimethylphosphine (358.8 mg, 3.48 mmol) were weighed into a Schlenk tube, and 5 mL toluene were added. The resulting dark orange solution was stirred at r.t. for one hour. This solution was added to a solution of [Hyp₃EtGe₃] (250 mg, 0.17 mmol) in 5 mL toluene. The brown reaction mixture was stirred at r.t. for 72 h. After filtration, the solvent was removed *in vacuo*, and the residue was washed with acetonitrile (3×5 mL). After drying in high vacuum, 192 mg of **4** (72%) were obtained as a brown solid. For crystallisation, a hexane solution of **4** was stored at −40 °C. Brown block-shaped crystals were obtained after 3 months.

¹H NMR (400 MHz, C₆D₆, 298 K): 0.35 (s, 54H, TMS), 0.68 (s, 27H, TMS), 1.34 (d, 9H, CH₃), 1.92 (br, 3H, CH₂CH₃), 2.73 (br, 2H, CH₂CH₃). ¹³C{¹H} NMR (100 MHz, C₆D₆, 298 K) 3.07 (TMS), 3.18 (TMS), 28.61 (CH₃). ³¹P{¹H} NMR (162 MHz, C₆D₆, 298 K): −12.81 (PMe₃@Ni). LIFDI/MS: *m/z* = 1560.44 [Hyp₃EtGe₃NiPMe₃]⁺, 1530.37 [Hyp₃Ge₃NiPMe₃]⁺, 1484.36 [Hyp₃EtGe₃Ni]⁺, 1455.30 [Hyp₃Ge₃Ni]⁺. Elemental analysis calc: C 24.63, H 6.14, Ni 3.76; found: C 25.75, H 5.79, Ni 3.34.

Isomerisation reactions—standard procedure

The respective catalyst (**1-4**) was placed in an NMR tube, the olefin (0.229 mmol) as well as 0.5 mL C₆D₆ were added immediately, finally the components were mixed by shaking the NMR tube. Subsequently, the reaction mixture was put into a preheated oil bath, and the reaction was monitored using ¹H and ³¹P NMR spectroscopy. After completion of the reaction, a GC/MS measurement was performed to confirm the products. The experiments performed this way are listed in Table 2.

Phosphine exchange reaction

Compound **1** (15 mg, 0.009 mmol) was placed in an NMR tube, and Triisopropylphosphine (2 mL, 0.009 mmol) as well as 0.5 mL C₆D₆ were added. Then the reaction mixture was put into a preheated oil bath, and the reaction was monitored using ³¹P NMR spectroscopy.

Supporting Information

The Supporting Information contains further details on the crystal structures of **3** and **4**, as well as NMR, LIFDI/MS and XPS spectra of compounds **1–4**. Also NMR spectra and calculations concerning the catalysis are provided.

The authors have cited additional references within the Supporting Information.^[60]

Acknowledgements

The authors are thankful for the financial support from *Wacker Chemie AG*. Peter Coburger thanks for financial support the Liebig fellowship of the VCI. They further thank B.Sc. Yasmina Boulesnam for the synthesis and preparations of different reaction solutions. Furthermore, we thank Ulrike Ammari and Petra Ankenbauer for the execution of the elemental analyses and Jürgen Kudermann for developing a suitable GC/MS method, Dr. Maximilian Muhr for performing the LIFDI/MS measurements, M.Sc. Rebecca Wilhelm for the XPS measurements and M.Sc. Kevin Frankiewicz for the help measuring the VT-NMR studies. Open Access funding enabled and organized by Projekt DEAL.

Conflict of Interests

The authors declare no conflict of interest.

Data Availability Statement

The data that support the findings of this study are available in the supplementary material of this article.

Keywords: cluster compounds · germanium · homogeneous catalysis · nickel · *Zintl* cluster

- [1] G. G. Hlatky, *Chem. Rev.* **2000**, 1347–1376.
- [2] Z. Li, D. Wang, Y. Wu, Y. Li, *Natl. Sci. Rev.* **2018**, *5*, 673–689.
- [3] J. D. Pelletier, J. M. Basset, *Acc. Chem. Res.* **2016**, *49*, 664–677.
- [4] J. M. Thomas, R. Raja, D. W. Lewis, *Angew. Chem. Int. Ed.* **2005**, *44*, 6456–6482.
- [5] B. Qiao, A. Wang, X. Yang, L. F. Allard, Z. Jiang, Y. Cui, J. Liu, J. Li, T. Zhang, *Nat. Chem.* **2011**, *3*, 634–641.
- [6] J. D. Corbett, D. G. Adolphson, D. J. Merryman, P. A. Edwards, F. J. Armatos, *J. Am. Chem. Soc.* **1975**, 6267–6268.
- [7] R. B. King, in *Zintl Ions: Principles and Recent Developments* (Ed.: T. F. Fässler), Springer Berlin Heidelberg, Berlin, Heidelberg, **2011**, pp. 1–24.
- [8] S. Scharfe, F. Kraus, S. Stegmaier, A. Schier, T. F. Fässler, *Angew. Chem. Int. Ed.* **2011**, *50*, 3630–3670.
- [9] C. Liu, Z.-M. Sun, *Coord. Chem. Rev.* **2019**, *382*, 32–56.
- [10] R. J. Wilson, N. Lichtenberger, B. Weinert, S. Dehnen, *Chem. Rev.* **2019**, *119*, 8506–8554.
- [11] T. F. Fässler, *Coord. Chem. Rev.* **2001**, *215*, 347–377.
- [12] C. Hoch, M. Wendorff, C. Röhr, *J. Alloys Compd.* **2003**, *361*, 206–221.
- [13] O. Kysliak, A. Schnepf, *Dalton Trans.* **2016**, *45*, 2404–2408.
- [14] F. Li, S. C. Sevov, *Inorg. Chem.* **2012**, *51*, 2706–2708.
- [15] S. Frischhut, T. F. Fässler, *Dalton Trans.* **2018**, *47*, 3223–3226.
- [16] S. Frischhut, W. Klein, M. Drees, T. F. Fässler, *Chem. Eur. J.* **2018**, *24*, 9009–9014.
- [17] F. Li, A. Munoz-Castro, S. C. Sevov, *Angew. Chem. Int. Ed.* **2012**, *51*, 8581–8584.
- [18] F. Li, S. C. Sevov, *J. Am. Chem. Soc.* **2014**, *136*, 12056–12063.
- [19] F. S. Geitner, T. F. Fässler, *Eur. J. Inorg. Chem.* **2016**, 2688–2691.
- [20] K. Mayer, L. J. Schiegerl, T. F. Fässler, *Chem. Eur. J.* **2016**, *22*, 18794–18800.
- [21] L. J. Schiegerl, M. Melaimi, D. R. Tolentino, W. Klein, G. Bertrand, T. F. Fässler, *Inorg. Chem.* **2019**, *58*, 3256–3264.
- [22] F. Henke, C. Schenk, A. Schnepf, *Dalton Trans.* **2009**, 9141–9145.
- [23] C. Schenk, F. Henke, G. Santiso-Quiñones, I. Krossing, A. Schnepf, *Dalton Trans.* **2008**, 4372–4386.
- [24] F. Li, S. C. Sevov, *Inorg. Chem.* **2015**, *54*, 8121–8125.
- [25] O. Kysliak, C. Schrenk, A. Schnepf, *Chem. Eur. J.* **2016**, *22*, 18787–18793.
- [26] O. Kysliak, D. D. Nguyen, A. Z. Clayborne, A. Schnepf, *Inorg. Chem.* **2018**, *57*, 12603–12609.
- [27] F. Henke, C. Schenk, A. Schnepf, *Dalton Trans.* **2011**, *40*, 6704–6710.
- [28] C. Schenk, A. Schnepf, *Chem. Commun.* **2009**, 3208–3210.
- [29] O. P. E. Townrow, C. Chung, S. A. Macgregor, A. S. Weller, J. M. Goicoechea, *J. Am. Chem. Soc.* **2020**, *142*, 18330–18335.
- [30] O. P. E. Townrow, S. B. Duckett, A. S. Weller, J. M. Goicoechea, *Chem. Sci.* **2022**, *13*, 7626–7633.
- [31] F. Li, A. Muñoz-Castro, S. C. Sevov, *Angew. Chem. Int. Ed.* **2016**, *55*, 8630–8633.
- [32] S. Frischhut, F. Kaiser, W. Klein, M. Drees, F. E. Kühn, T. F. Fässler, *Organometallics* **2018**, *37*, 4560–4567.
- [33] Y. Heider, D. Scheschkewitz, *Dalton Trans.* **2018**, *47*, 7104–7112.
- [34] N. E. Poitiers, L. Giarrana, V. Huch, M. Zimmer, D. Scheschkewitz, *Chem. Sci.* **2020**, *11*, 7782–7788.
- [35] C. A. Tolman, *Chem. Rev.* **1977**, *77*, 313–348.
- [36] L. S. Meriwether, J. R. Leto, *J. Am. Chem. Soc.* **1961**, *83*, 3192–3196.
- [37] G. Pacchioni, P. S. Bagus, *Inorg. Chem.* **1992**, *31*, 4391–4398.
- [38] Deposition Numbers 2172747 (for **3**) and CCDC 2171746 (for **4**) contain the supplementary crystallographic data for this paper. These data are provided free of charge by the joint Cambridge Crystallographic Data Centre and Fachinformationszentrum Karlsruhe Access Structures service.
- [39] H. Kanai, K. Kushi, K. Sakanoue, N. Kishimoto, *Bull. Chem. Soc. Jpn.* **1980**, *53*, 2711–2715.
- [40] J. Zhang, H. Gao, Z. Ke, F. Bao, F. Zhu, Q. Wu, *J. Mol. Catal. A* **2005**, *231*, 27–34.
- [41] H.-W. Suh, L. M. Guard, N. Hazari, *Polyhedron* **2014**, *84*, 37–43.
- [42] T. F. C. Cruz, P. S. Lopes, P. T. Gomes, *Polyhedron* **2021**, *207*, 115357.
- [43] G. R. Fulmer, A. J. M. Miller, N. H. Sherden, H. E. Gottlieb, A. Nudelman, B. M. Stoltz, J. E. Bercaw, K. I. Goldberg, *Organometallics* **2010**, *29*, 2176–2179.
- [44] *MestreNova*, version 14.2.2; Mestrelab Research, **2021**.
- [45] *X-Area*, version 1.76.8.1; Stoe & Cie GmbH: Darmstadt, Germany, **2015**.
- [46] G. M. Sheldrick, *Acta Crystallogr. Sect. C* **2015**, *71*, 3–8.
- [47] C. B. Hübschle, G. M. Sheldrick, B. Dittrich, *J. Appl. Crystallogr.* **2011**, *44*, 1281.
- [48] A. L. Spek, *Acta Crystallogr.* **2009**, *D65*, 148–155.
- [49] *Diamond Version 3.2k*, Crystal Impact GbR, **2014**.
- [50] F. Neese, *Wiley Interdiscip. Rev.: Comput. Mol. Sci.* **2018**.
- [51] F. Neese, F. Wennmohs, U. Becker, C. Riplinger, *J. Chem. Phys.* **2020**, *152*.
- [52] R. A. Kendall, H. A. Früchtl, *Theor. Chem. Acc.* **1997**, *97*, 158–163.
- [53] E. Caldeweyher, C. Bannwarth, S. Grimme, *J. Chem. Phys.* **2017**, *147*.
- [54] S. Grimme, J. Antony, S. Ehrlich, H. Krieg, *J. Chem. Phys.* **2010**, *132*.
- [55] S. Grimme, S. Ehrlich, L. Goerigk, *J. Comput. Chem.* **2011**, *32*, 1456–1465.
- [56] F. Weigend, R. Ahlrichs, *Phys. Chem. Chem. Phys.* **2005**, *7*, 3297–3305.
- [57] J. Tao, J. P. Perdew, V. N. Staroverov, G. E. Scuseria, *Phys. Rev. Lett.* **2003**, *91*, 146401.
- [58] M. Muhr, P. HeiB, M. Schütz, R. Bühler, C. Gemel, M. H. Linden, H. B. Linden, R. A. Fischer, *Dalton Trans.* **2021**, *50*, 9031–9036.
- [59] *CasaXPS*, version 2.3.25; Casa Software Ltd, **2022**.
- [60] J. F. Moulder, W. F. Stickle, P. E. Sobol, K. D. Bomben, *Handbook of X-ray photoelectron spectroscopy*, Perkin-Elmer Corporation, Minnesota, **1992**.

Manuscript received: October 12, 2023
 Revised manuscript received: November 3, 2023
 Accepted manuscript online: November 6, 2023
 Version of record online: December 4, 2023